Journal of Applied Polymer Science

Numerical and experimental studies for gas assisted extrusion forming of molten polypropylene

Zhong Ren,[1,2] Xingyuan Huang,[1] Hesheng Liu,[1] Xiaozhen Deng,[1] Jiantao He[1]
[1]College of Mechanical and Electrical Engineering, Nanchang University, Nanchang 330031, China
[2]Key Laboratory of Optic-electronic and Communication, Jiangxi Science and Technology Normal University, Nanchang 330038, China
Correspondence to: X. Huang (E-mail: huangxingyuan001@126.com)

ABSTRACT: In this study, the experiments of gas-assisted extrusion (GAE) for molten polypropylene were carried out under different gas pressures, the different extrudate deformations and sharkskin defects of melt were observed. To ascertain the effects of gas on melt extrusion, non-isothermal numerical simulation of GAE based on gas/melt two-phase fluid model was proposed and studied. In the simulations, the melt extruded profile, physical field distributions (velocities, pressure drop, and first normal stress difference) were obtained. Numerical results showed that the deformation degree of melt increased with increasing gas pressure, which was in good agreement with experimental results. It was demonstrated that the influence of gas pressure on the melt extrusion could be well reflected by GAE simulation based on gas/melt two-phase fluid model rather than simplified-GAE (SGAE) based on full-slip wall boundary condition used in the past time. Experimental and numerical results demonstrate that the gas pressure induced first normal stress difference is the main reason of triggering flow behavior changes, extrudate deformations, and sharkskin defects of melt. Therefore, the reasonable controlling of gas pressure is a key in practice of GAE, and the gas layer and its influence should be considered in GAE numerical simulation. © 2015 Wiley Periodicals, Inc. J. Appl. Polym. Sci. **2015**, *132*, 42682.

KEYWORDS: extrusion; molding; rheology; theory and modeling; viscosity and viscoelasticity

Received 4 May 2015; accepted 1 July 2015
DOI: 10.1002/app.42682

INTRODUCTION

Extrusion forming[1,2] is a polymer processing method, which has widely been applied into a variety of plastic products such as rods,[3] pipes,[4] films,[5] profiled plastics,[6] etc. It was reported that the plastic production of extrusion had accounted for nearly 40% of all the plastic productions in the world. But in the process of extrusion, the extrudate swell,[7–10] melt fracture,[11,12] and extrusion distortion phenomena[13] are often observed. Apart from the material viscoelasticity, die geometric structure, and process parameters, the stick-slip effect between the melt and the die was also studied by many researchers.[14–17] Up to now, some methods such as fluoropolymer,[18] additive,[19] vibration extrusion,[20,21] etc. have been used to improve the stick-slip effect between the melt and the die. Gas-assisted extrusion (GAE) of molten polymer is a good and promising forming technique because the extrusion problems can be greatly eliminated by means of gas layer established between the melt and the die. Brzoskowski *et al.*[22] firstly introduced the air-lubricated technique into the extrusion of rubber compounds. Liang *et al.*[23] firstly used the nitrogen gas-assisted method into the extrusion experiments of molten polyethylene. Kamişli[24] studied the gas-assisted fluid behavior in a circular tube and a rectangular channel. Huang[25] established the experimental device of gas-assisted rod polymer extrusion via a single screw extruder and a designed dies. Up to now, many experimental and simulation researches[22–31] have demonstrated that GAE can overcome the extrusion problems due to the elimination of pressure drop, shear stress and normal stress difference of molten polymers. Huang *et al.*[25,26] undertook the simulation of GAE via the finite element method based on Rivlin-Ericksen viscoelastic constitutive model, and studied the influence factors and the stability of gas layer in the experiment of GAE, his research results verified that the extrudate swell phenomenon, pressure drop, and shear stress were eliminated by gas-assisted method. Liu *et al.*[27] numerically and experimentally found the extrudate swell of T profiled polymer was eliminated and the extruded shape could be accurately controlled. Xiao *et al.*[28] found that the GAE method greatly eliminated the pressure drop and stress concentration. Huang[29] carried out the simulation and experimental studies of GAE for two layers of polymer with square cross-section, he verified that the extrudate swell, interfacial instability, and pressure drop were well eliminated via gas-assisted

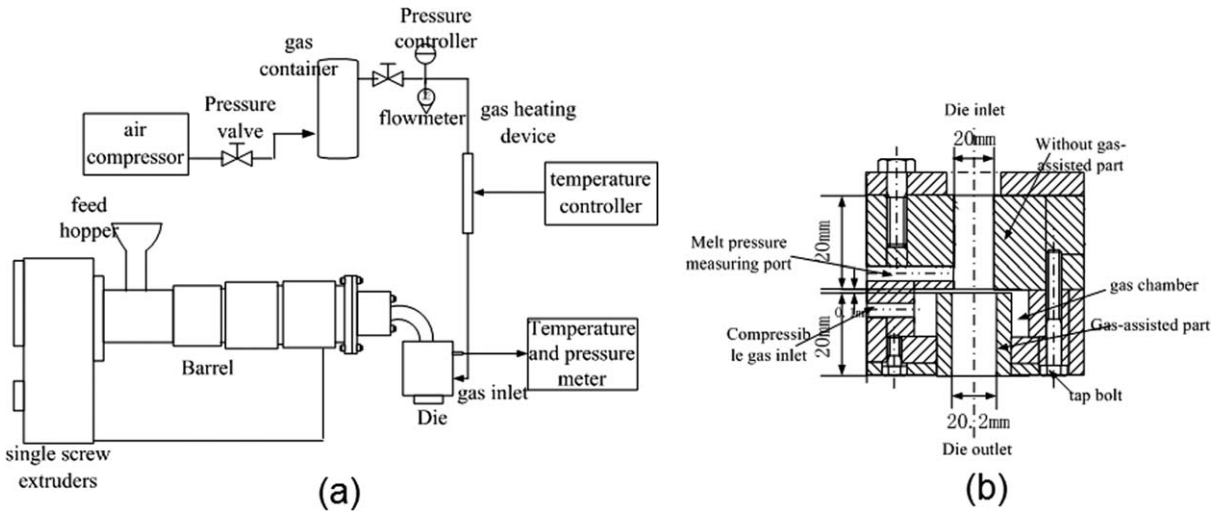

Figure 1. Experimental setup (a) and designed die (b).

method. Deng *et al.*[30] undertook the numerical and experimental studies on the GAE for two layers of L-profiled polymer, she found that GAE effectively diminished the die swell, encapsulation, and interfacial instability phenomenon. However, Arda *et al.*[31] experimentally found that the sharkskin instabilities were not completely removed in the GAE, and numerical results demonstrated that the stress concentration at the exit of die was transferred to the import of gas injection. But up to now, the flow behaviors, extrudate deformations, and instabilities of melt in GAE have not been well presented in the numerical simulations. In the past years, the numerical simulations of GAE were achieved via a simplified method of full-slip wall boundary condition,[23,25–31] that is, the wall-slip coefficient is set to zero in Navier's slip law, or the normal velocity and tangential stress are all set to zero on the interface between the melt and wall. Although the seemingly satisfying extrudate profiles of melt can be obtained using this simplified method, the influences of the gas on the real physical field distributions and flow behaviors of the melt are not considered, which leads to the obvious deviations between the numerical results and the experimental results.

This study has four main objectives. Firstly, experimentally studying the influence of gas pressure on melt extrusion forming. The GAE experiments of molten polyethylene with a given volumetric flow rate and temperature under different gas pressures were carried out. In the experiments, the extrudate shapes and surface qualities change of melt under the different gas pressures are investigated. Secondly, in order to as much as possible represent actual flow behaviors, physical field distributions (flow velocities, pressure drop, and first normal stress difference), and extrudate profile changes of melt, a modified GAE (MGAE) numerical simulation based on gas/melt two-phase fluid model was proposed instead of the full-slip wall boundary condition using a commercial finite element CFD package POLYFLOW.[32] And the changeable gas density is taken into account because of gas compressibility. The third objective of this study is to reveal the drawback of SGAE simulation method based on full-slip wall boundary condition by using MGAE simulation method based on the gas/melt two-phase fluid model. The fourth objective is to ascertain the influence mechanism of gas on melt extrusion.

EXPERIMENTAL

Experimental Setup and Material

In this study, the experimental material of polymer used was polypropylene (PP) (5018T, Yongjia Co., Taiwan), its density is 900 kg/m^3 and melt flow index is 1.7 g/10 min. The experiments of GAE were carried out by using a single screw extruders (SJ-65/5.5kW). The screw length-to-diameter ratios is 24.6, and the screw diameters is 65 mm, respectively. The gas-assisted system consists of the air compressor (0G06F, GAIRS Co., Shanghai, China), high pressure gas container (1V-3/8, Nanchang, China), pressure reduction valve (QTY-15, Quansheng Automation Engineering Co., Fenhua, China), flowmeter (LZB-40, Yinhuan Co., Yuyao, China), pressure controller, gas heating device, and gas tube etc. where, the air compressor is the single screw air-cooled series air compressor, its gas exhaust volume can reach 0.8 m^3/min, the maximum output pressure can reach 0.7 MPa. The volume of the high-pressure gas container is 0.4 m^3, which is used to decrease the gas pressure fluctuation. The gas-heating device consists of the electric heating wire, copper tube, and temperature controller (XMT-001, Jiaming Instrument Co., Xinghua, China). To heat the compressible gas, the electric heating wire is wound on the copper tube, and in order to prevent leakage, the heating wire is tied by the ceramic tube. In addition, to decrease the gas temperature instability, the copper tube is bound by the mineral wool and glass cloth. The experimental setup is shown in Figure 1(a). In this study, the die of GAE was designed as shown in Figure 1(b), which consisted of the confluence section, traditional extrusion section and gas-assisted extrusion section. The gas gap between the traditional extrusion section and the gas-assisted extrusion section is about 0.1 mm.

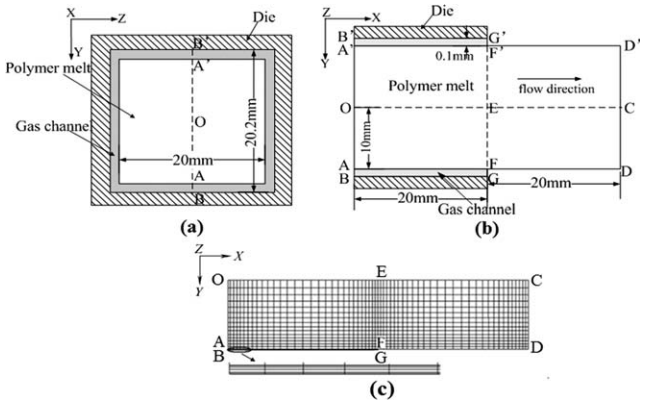

Figure 2. Geometry model and finite element mesh of MGAE based on gas/melt two-phase fluid. (a) Cross-section of model, (b) axis-section of model, and (c) finite element mesh.

Process Parameters and Basic Procedure of GAE Experiments

In the experiments of GAE, the temperature of gas was controlled about 200°C. The temperature of the polymer melt and the die were detected by the pressure/temperature sensor (PT131, Wuyue Co, Xiaogan, China), the temperature of polymer melt and die were all controlled about 190°C. The screw speed of the extruder was set to 4.46 rpm. The pressure of polymer melt was about 0.1 MPa.

The experimental basic procedure is given as follows: firstly, heating the feeding section, melting section, homogeneous section of the extruder and the die, controlling the temperature of the die reaches 190°C. Secondly, opening the gas valve of the high pressure gas container, the gas is heated by means of the gas heating device, and transmitted into the gas chamber via the gas tube, then the heated gas passes through the gas gap and enters into the die and gas channel. Thirdly, turning on the extruder to control the screw speed and loading the polypropylene into the barrel of extruder from feed hoper to begin the GAE experiment. In the experiments, in order to form the gas-assisted layer and investigate the influence of the gas pressure on the melt extrusion, the gas pressure was slowly increased from 0 MPa to 0.4 MPa.

NUMERICAL SIMULATION

GAE Models Based on Gas/Melt Two Phase Fluid

The two dimension geometry models and finite element mesh of MGAE based on gas/melt two-phase fluid are shown in Figure 2. The size of this geometry model is consistent with that of the experiments. Figure 2(a) is the cross section of the model. The integrated width of die channel is 20.2 mm, where the width of polymer melt is 20 mm, and the width of gas channel is 0.1 mm. Figure 2(b) is the axial section of the model. In Figure 2(b), $ADD'A'$ is polymer melt zone, where $AFF'A'$ is melt zone inside the die, $FDD'F'$ is melt zone outside the die, $ABGF$ and $A'B'G'F'$ are the gas channel inside the die. In the two-phase fluid model, AA' and FF' is the inlet and outlet of the die, respectively. AB, $A'B'$ and FG, $F'G'$ are the inlet and outlet of gas channel, respectively. DD' is the exit of melt, OC is symmetry axis. The length of die and gas channel are all equal to 20 mm, the length of external melt is also 20 mm.

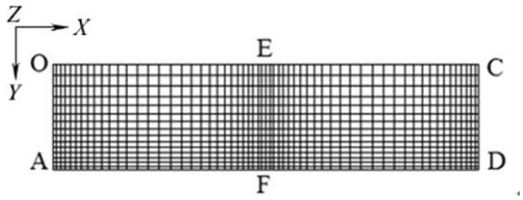

Figure 3. Geometry model and finite element mesh of SGAE and WGAE.

Since the geometric structure of axial section for the gas/melt two-phase fluid model is symmetric, a half of model is used in numerical simulations in order to save the computing time. The finite element mesh of the half of model is shown in Figure 2(c). In the mesh, the quadrilateral structural mesh was used in the grid division. To guarantee the accuracy of simulation results, the meshes are refined close to the inlet boundaries, outlet boundaries of polymer melt and gas channel and the gas/melt interface, the mesh number of Figure 2(c) is 1080. In Figure 2(c), the amplified local mesh at the entrance of gas channel is presented at the bottom of the two-phase fluid mesh.

In this study, to verify the numerical availability of MGAE based on gas/melt two-phase fluid model, the numerical simulation of SGAE based on the full-slip wall boundary condition and WGAE based on non-slip boundary condition were also performed. For both of them, the gas channel was removed from Figure 1 because the full-slip or non-slip boundary conditions were used. The geometry model and finite element mesh of the SGAE and WGAE are shown in Figure 3. The mesh number of Figure 3 is 900.

Governing Equations and Constitutive Equations

According to the flow characteristics of polymer melt and gas in the GAE, we made the following several hypotheses to perform the numerical simulation. (1) Polymer melt is regarded as the incompressible non-Newtonian viscoelastic fluid, but gas is regarded as the compressible Newtonian fluid; (2) The flow of the polymer melt and gas are all fully developed steady laminar flow, the turbulent effect of gas is neglected. The non-isothermal effect dependent of the temperature is taken into consideration because the flow velocity of polymer melt is relatively slow and the compressibility of gas is dependant on the local temperature; (3) The inertia, gravity force, and surface tension of polymer melt and gas are neglected because of the high viscosity and slow velocity characteristics of polymer melt, at the same time, low viscosity and density of the gas; and (4) The stick-slip effects between the gas and the melt as well as the die are neglected.

Based on the above mentioned reasonable hypotheses, the polymer process rheology and gas dynamics, the governing equations are presented as follows:

$$\text{Continuity equation}: \nabla \cdot (\rho_k u_k) = 0, \quad k = I, \text{II} \tag{1}$$

$$\text{Momentum equation}: \rho_k u_k \cdot \nabla u_k + \nabla p_k - \nabla \cdot \tau_k = 0, \quad k = I, \text{II} \tag{2}$$

Energy equation:

$$\begin{cases} \rho_k C_{pk} u_k \cdot \nabla T_k - k_k \cdot \nabla^2 T_k = \tau_k : \nabla u_k & k=I \\ \rho_k C_{pk} u_k \cdot \nabla T_k - k_k \cdot \nabla^2 T_k = -p_k \nabla u_k \delta_k + \tau_k : \nabla u_k, & k=I\,I \end{cases} \tag{3}$$

where $k=I$, II denotes melt phase and gas phase, respectively. ∇ is Hamilton operator, u_k is velocity vector, p_k is pressure drop,τ_k is stress tensor, k_k is thermal conductivity, C_{pk} is specific heat capacity at constant volume, T_k is absolute temperature of the fluids. ρ_k is density of fluids. In the governing equations, for the melt phase, its density is constant because it is regarded as incompressible fluid, but for gas, its density is a variant because it is regarded as the compressible fluid.

In this study, Phan-Thien and Tanner (PTT) constitutive model[33] was selected as the viscoelastic constitutive equation because it not only exhibits shear thinning characteristics like the purely-viscous fluid, but also better describes the viscoelastic effect related to normal stress and stress relaxation, PTT differential viscoelastic constitutive model is shown as follows:

$$\tau_I = \tau_{I1} + \tau_{I2} \tag{4}$$

$$\exp\left[\frac{\varepsilon\lambda}{(1-\eta_{Ir})\eta_I} tr(\tau_{I1})\right]\tau_{I1} + \lambda\left[\left(1-\frac{\xi}{2}\right)\tau_{I1}^{\nabla} + \frac{\xi}{2}\tau_{I1}^{\Delta}\right] = 2(1-\eta_{Ir})\eta_I \mathrm{D}_I \tag{5}$$

$$\tau_{I2} = 2\eta_{I2}\mathrm{D}_I \tag{6}$$

where τ_I is the total extra-stress tensor of the melt, τ_{I1} is the melt viscoelastic component of the total extra-stress tensor (τ_I), τ_{I2} is the melt purely-viscous component of total extra-stress tensor (τ_I), η_I is total viscosity of polymer melt, $\eta_{Ir}=\eta_{I2}/\eta_I$ is the viscosity ratio, η_{I1} is model-specific viscosity factor for the viscoelastic component of total extra-stress tensor (τ_I), η_{I2} is viscosity factor for the Newtonian (i.e. purely-viscous) component of the total extra-stress tensor (τ_I), λ is a model-specific relaxation time, ξ and ε are material properties controlling the shear viscosity and elongational behavior of polymer melt, respectively. D_I is the melt rate-of-deformation tensor, which is equal to $D_I=\frac{1}{2}(\nabla u_I+\nabla^T u_I)\cdot\tau_{I1}^{\nabla}$ and τ_{I1}^{Δ} is the upper-convected and below-convected time derivative of the viscoelastic extra stress tensor (τ_I), respectively, which are defined as follows:

$$\tau_{I1}^{\nabla} = \frac{\mathrm{D}\tau_{I1}}{\mathrm{D}t} - \tau_{I1}\cdot\nabla v_I - \nabla v_I{}^T\cdot\tau_{I1} \tag{7}$$

$$\tau_{I1}^{\Delta} = \frac{\mathrm{D}\tau_{I1}}{\mathrm{D}t} + \tau_{I1}\cdot\nabla v_I{}^T + \nabla v_I\cdot\tau_{I1} \tag{8}$$

Since the gas is regarded as the Newtonian fluid, the viscoelastic component is zero, its constitutive equation can be given as follows:

$$\tau_{II} = 2\eta_{II}\mathrm{D}_{II} - \frac{2}{3}\eta_{II}\nabla u_{II}\delta_{II} \tag{9}$$

where η_{II} is the Newtonian shear viscosity of gas, D_{II} is the rate-of-deformation tensor of gas, which is equal to $D_{II}=\frac{1}{2}(\nabla u_{II}+\nabla^T u_{II})$; δ_{II} is two order unit tensor of Kronecker, that is, $\delta_{ij}=\begin{cases}1 & i=j\\ 0 & i\neq j\end{cases}$.

For the non-isothermal flow, the temperature dependence of the viscosity must be taken into account together with the shear rate dependence. The temperature-dependant viscosity law can be expressed as follows:

$$\eta_k = \eta_{0k}(\dot{\gamma}_k)\cdot\boldsymbol{H}(T_k) \tag{10}$$

where $\boldsymbol{H}(T_k)$ is the Arrhenius law, $\eta_{0k}(\dot{\gamma}_k)$ is the viscosity law at the reference temperature (T_{rk}).

The Arrhenius-law equation is given as follows:

$$H(T_k) = \exp\left[\alpha_k\left(\frac{1}{T_k-T_0}-\frac{1}{T_{rk}-T_0}\right)\right] \tag{11}$$

where α_k is the energy of activation coefficient of the fluid (K), T_{rk} is a reference absolute temperature for which $\boldsymbol{H}(T_k)=1$. The reference absolute temperature (T_0) is set to zero.

The ideal gas state equation is used to solve the gas density and the closure equations of gas, which is given as follows:

$$p_{II} = \rho_{II} R T_{II} \tag{12}$$

where p_{II} is gas local pressure, T_{II} is gas local temperature, R is gas constant (287 J/kg·K). The ideal gas state equation is implemented by using the UDF method[32] in the finite element CFD package POLYFLOW coupled with CLIPS programming.

Boundary Conditions

For all boundaries, the normal force (f_n), tangential force (f_s), normal velocity (v_n), and tangential velocity (v_s) are mainly taken into account. According to the geometric model in Figure 2, the flow boundary conditions and temperature boundary conditions are set to as follows:

1. Inlet boundary: We imposed the fully developed flow condition at the inlet of the melt phase and gas phase, the dynamic condition is shown as follows:

$$\partial v_x/\partial x = 0,\ v_y = 0 \tag{13}$$

where v_x and $r=R$ are fluid velocities at the axial and radial direction of die channel, respectively. The coordination$x$ is the flow direction of melt and gas.

In the numerical simulation of this study, the inflow volumetric flow rate of melt was set to 1.0×10^{-6} m^3/s. The normal pressure was imposed on the inlet boundary of gas. For the thermal boundary condition, the inlet temperature boundary of melt was set to 190°C. According to the experimental results of Huang *et al.*,[25,26] it was found that the gas layer could be well established only when the temperature of gas was equal to or higher than that of melt. So, the inlet temperature of gas was set to 200°C.

2. Wall boundary: Supposing that there is non-slip between the gas and the wall, the dynamic condition is given as follows:

$$v_n = v_s = 0 \tag{14}$$

For the thermal boundary condition, the constant wall temperature is used, the temperature of wall was set to 190°C as same as that of the melt.

Table I. Material Parameters of Polymer Melt and Compressible Air

Parameters	PP	Compressible air
Total viscosity η_k/(Pa·s)	8823	2.6×10^{-5}
Relaxation time λ/(s)	0.1	0
ε	0.15	0
ξ	0.44	0
Viscosity ratio (η_r)	0.12	0
Thermal conductivity k_k/(W/m·°C)	0.22	0.037
Specific heat capacity C_{pk}/(J/Kg·°C)	1883	1026
Temperature T_k/(°C)	190	200

3. Symmetric boundary: Since that the flow, temperature and heat flux of fluids are continuous across the symmetric boundary, the flow and temperature kinematic and dynamic conditions of the symmetric boundary should obey the following equations:

$$f_s=0,\ v_n=0,\ \text{and}\ T_i=T_j \tag{15}$$

where i, j are two infinite short regions oppositely distanced from the symmetric axis.

4. Gas/melt interface: Neglecting the surface tension and the relative slip on the interface between the gas and the melt. And the normal and tangential stresses of two fluids are balanced on the gas/melt interface, and without fluids passing through the interface. So, the kinematic and dynamic conditions should obey the following equations:

$$f_{In}=f_{IIn}, f_{Is}=f_{IIs} \tag{16}$$

$$v_{Is}=v_{IIs}, \vec{v}\cdot\vec{n}=0 \tag{17}$$

where $\vec{n}$ is the normal unit vector.

The thermal boundary condition of gas/melt interface as same as that of the symmetric boundary.

5. Free boundary: Neglecting the surface tension on the free surface, and no force is imposed and no flow across the free surface, the kinematic and dynamic conditions are given as follows:

$$f_n=0,\ f_s=0\ \text{and}\ v_n=0, \vec{v}\cdot\vec{n}=0 \tag{18}$$

For free boundary, the heat flux condition was imposed on the free boundary because the heat convection exchange takes place between the polymer melt and the outside environment, and the heat radiation effect was neglected. The heat convection exchange equation is given as follows:

$$q=-k\nabla T=\alpha(T-T_a) \tag{19}$$

where q is heat flux; k is thermal conductivity; α is the local heat convection coefficient, which is depend on the Prandtl and Reynold number in general, according to the empirical value of natural air convection, its value was set to about 5 W/m^2·K in this study; T_a is the ambient temperature, its value was set to about 27°C.

6. Exit boundary: Supposing that without traction forces are imposed on the exit boundaries, so, the normal stress and tangential velocity are assumed to be zero, i.e.

$$f_n=0\ \text{and}\ v_s=0 \tag{20}$$

For the thermal boundary of melt and gas exit, the outflow thermal condition is imposed because of unknown temperature in advance.

Material Parameters

In the numerical simulation of GAE, the material parameters of PP[30] and compressible air of numerical simulation are listed in Table I.

RESULTS AND DISCUSSION

Experimental Results

Influence of Gas Pressures on the Melt Shape. In the experiments, in order to verify the availability of the numerical simulation of MGAE based on gas/melt two-phase fluid model and to ascertain the influence of the gas pressure on the melt extrusion, the gas pressure was slowly increased from 0 MPa to 0.4 MPa. Figure 4(a–d) show the extruded melt shapes for the gas pressure of 0 MPa, 0.1 MPa, 0.2 MPa, and 0.4 MPa, respectively.

From Figure 4(a), it can be seen that the obvious extrudate swell phenomenon is generated when the gas pressure is less than that of melt. When the gas pressure is increased to 0.1 MPa, the stable gas-assisted layer can be established, and the extruded melt is not deformed (see Figure 4(b)). But in Figure 4(c), when the gas pressure is continued to increase, the gas-assisted extrusion instability phenomenon is generated. When the gas pressure reaches 0.2 MPa, the obvious melt fracture (waviness phenomena) is generated. And the melt fracture becomes more serious when the gas pressure is continuously increased. From Figure 4(d), it can be seen that the serious distortion phenomenon is generated when the gas pressure reaches

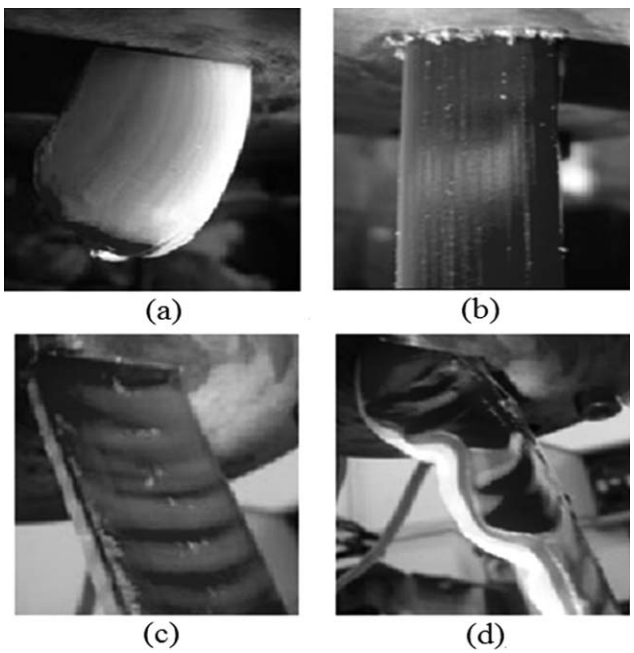

Figure 4. Experimental results of GAE polymer melt. (a) Gas pressure is 0 MPa, (b) gas pressure is 0.1 MPa, (c) gas pressure is 0.2 MPa, and (d) gas pressure is 0.4 MPa.

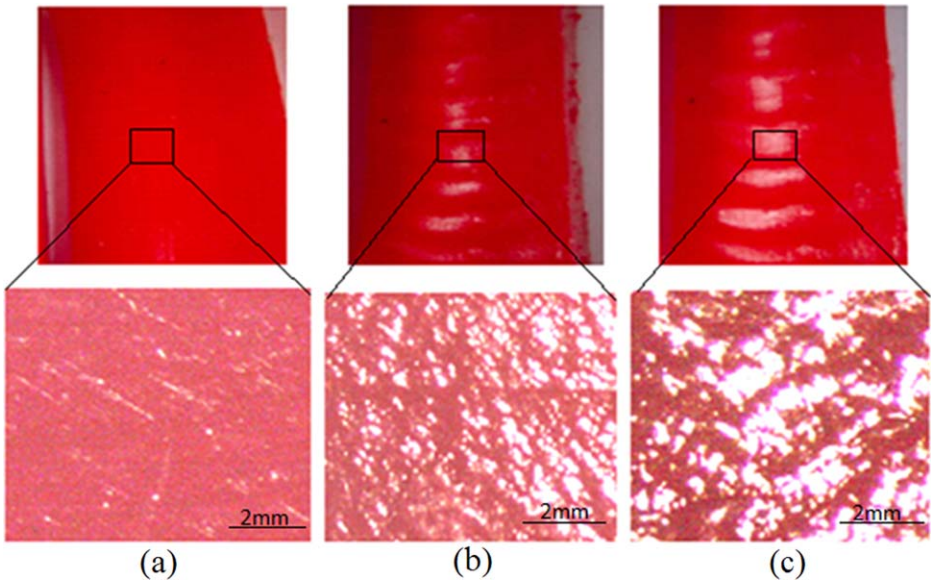

Figure 5. Macro and local amplified two times surface quality of melt for the different gas pressures. (a) Gas pressure is 0.1 MPa, (b) gas pressure is 0.2 MPa, and (c) gas pressure is 0.3 MPa. [Color figure can be viewed in the online issue, which is available at wileyonlinelibrary.com.]

0.4 MPa. And the melt can be blowing-broken by compressible gas when the gas pressure exceeds 0.4 MPa.

Influence of the Gas Pressure on the Melt Surface Quality. In order to know the influence of the gas pressure on the melt surface quality, the extruded melt surface was photographed by a camera (DSC-W55, SONY Co., Japan). The macro morphology and the surface quality photos amplified two times of extruded melt under the gas pressure of 0.1, 0.2, and 0.3 MPa are shown in Figure 5(a–c), respectively.

From Figure 5, it can be seen that the melt surface is good when the gas pressure is about 0.1 MPa (see Figure 5(a)). But when the gas pressure is continuously increased, from Figure 5(b,c), it can be seen that the obvious extrudate sharkskin or waveness phenomena are generated. And From the local amplified two times surface quality of Figure 5, it can also be seen that the melt surface of extruded melt becomes rougher and rougher.

Numerical Results

Influence of Gas Pressures on the Melt Shape. To ascertain the influence of the compressible gas on the polymer melt extrusion, four different gas pressures (0.101 MPa, 0.111 MPa, 0.151 MPa, and 0.201 MPa) were respectively used in the numerical simulations, these four gas pressures are identical to the practical values in experiments.

Figure 6(a–d) show the melt extruded shapes of MGAE under the influence of four different gas pressures of 0.101, 0.111, 0.151, and 0.201 MPa, respectively.

Figure 7 shows the extrudate shrinkage ratios of melt under four different gas pressures. Meanwhile, the mesh independency check is performed to make sure that result is independent to

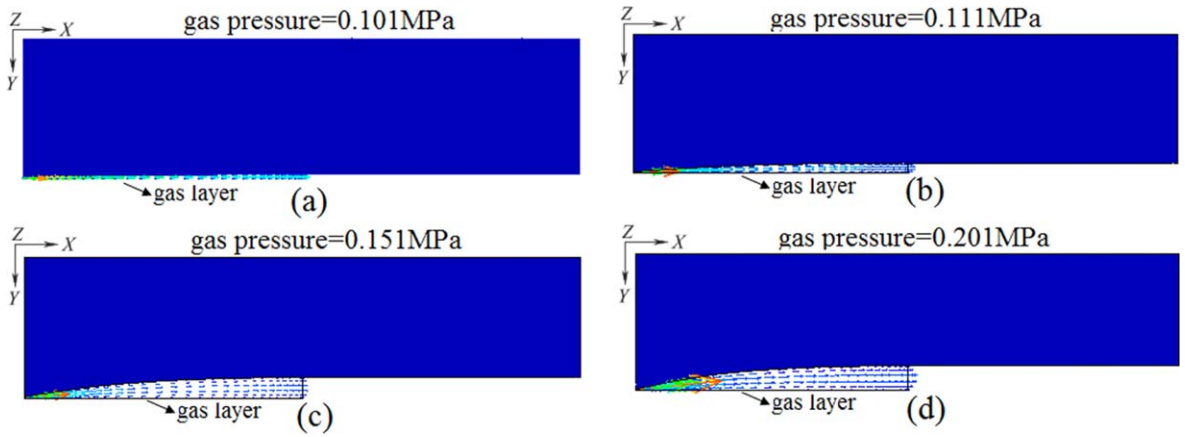

Figure 6. Melt extruded shapes of MGAE based on two-phase fluid model under different gas pressures. [Color figure can be viewed in the online issue, which is available at wileyonlinelibrary.com.]

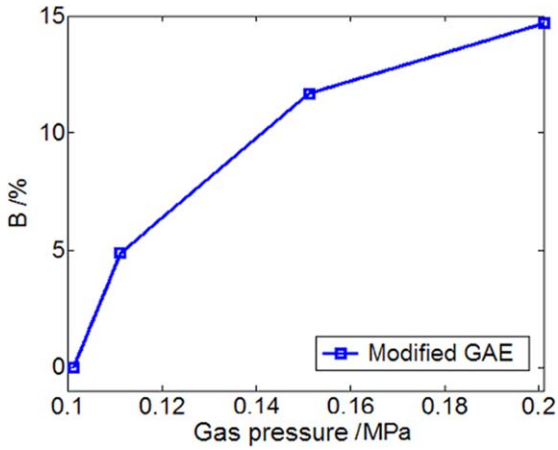

Figure 7. The extrudate shrinkage ratios of melt. [Color figure can be viewed in the online issue, which is available at wileyonlinelibrary.com.]

mesh size. The extrudate shrinkage ratio of melt can be computed based on the following equation:

$$\boldsymbol{B}=[(\boldsymbol{S}_0-\boldsymbol{S}_1)/\boldsymbol{S}_0]\times 100\% \quad (21)$$

where $\boldsymbol{B}$ is the shrinkage ratio, $\boldsymbol{S}_0$ is the area of *OADC* (see Figure 2(b)), and $\boldsymbol{S}_1$ is the shrinked area.

From Figures 6 and 7, it can be seen that the melt shape does not change when the gas pressure is about 0.101 MPa, but the shrinkage degree of melt increases with increasing the gas pressure.

Figure 8(a,b) show the melt shape of WGAE and SGAE, respectively. From Figure 8(a,b), it can be seen that the extrudate swell phenomenon of WGAE is obvious, but the melt shape of SGAE does not change at the same inflow volumetric flow rate of the melt.

Influence of Gas Pressures on the Flow Velocities of Melt. *X velocity distributions of melt.* To know the flow behaviors of melt, the flow velocities of MGAE based on two-phase fluid model with four different gas pressures were obtained and compared with that of WGAE and SGAE.

Figure 9(a–d) show the melt X velocity distributions of MGAE for the four gas pressure. Figure 9(e,f) show the melt X velocity distributions of WGAE and SGAE, respectively. Figure 9(g,f) show the melt X velocity changes of WGAE, SGAE, and four MGAEs along the axial direction of the die channel and the radial direction of the die entrance, respectively.

From Figure 9(a–d,g), it can be seen that the melt X velocity increases with increasing the gas pressure, and for each gas pressure, the melt axial X velocity also gradually increases along the direction of die channel. Moreover, In Figure 9(h), the melt radial X velocity along the radial direction of die entrance also increases with increasing the gas pressure, and for each gas pressure, the melt radial X velocity adjacent to the gas/melt interface is higher than that of the inner melt. So, it is found that the melt X axial and radial velocities increase under the influence of the compressible gas assisted.

For the WGAE [see Figure 9(e,g,h)], it can be seen that the melt X axial velocity along the direction of die channel gradually decrease in "S" shape, and the melt X radial velocity along the radial direction of die entrance gradually decreases to zero in the form of parabolic curve, that is, the melt X radial velocity adjacent to the die wall is lower than that of the inner melt. So, the melt X velocity of WGAE is opposite to that of the MGAE. However, for the SGAE [see Figure 9(f,g,h)], the melt X velocity is not changed.

Y velocity distributions of melt.. Figure 10(a–d) show the melt Y velocity distributions of MGAE corresponding to the four different gas pressures. Figure 10(e,f) show the melt Y velocity distributions of WGAE and SGAE, respectively. Figure 10(g) and (h) show the melt Y velocity changes of WGAE, SGAE, and four MGAEs along the axial direction of die channel and the radial direction of die entrance, respectively.

From Figure 10(a–d,g), it can be seen that the melt axial Y velocity is negative at the die entrance and increases with increasing the gas pressure. Moreover, in Figure 10(h), the melt radial Y inverse velocity along the radial direction of die channel also increases with increasing the gas pressure. And for each of gas pressure, the melt radial Y inverse velocity increases along the radial direction of the die entrance, that is, the melt radial Y inverse velocity adjacent to the gas layer is higher than that of the inner melt. So, it is also illustrated that the melt axial and radial Y velocities also increase under the influence of the compressible gas-assisted.

For the WGAE [see Figure 10(e,g,h)], the melt Y velocity is changed at the die exit, and the Y positive velocity is very large. So, it is demonstrated that the melt has the positive radial flow behavior and the radial extrudate swell phenomenon at the die exit. For the SGAE [see Figure 10(f,g,h)], the melt Y velocity is also not changed as same as X velocity, which is obviously not consistent with the actual situation of GAE.

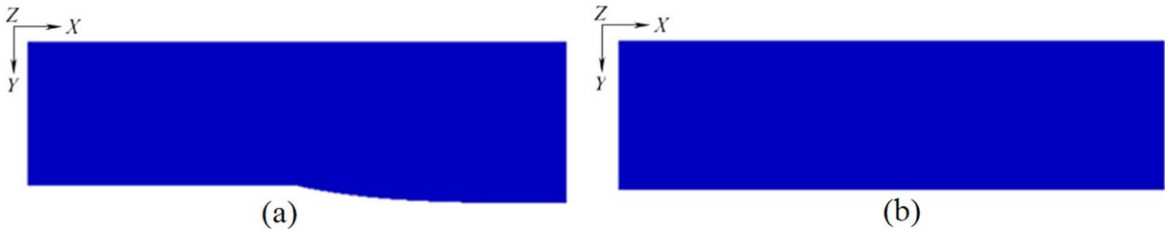

Figure 8. The melt extruded shape of WGAE (a) and SGAE (b). [Color figure can be viewed in the online issue, which is available at wileyonlinelibrary.com.]

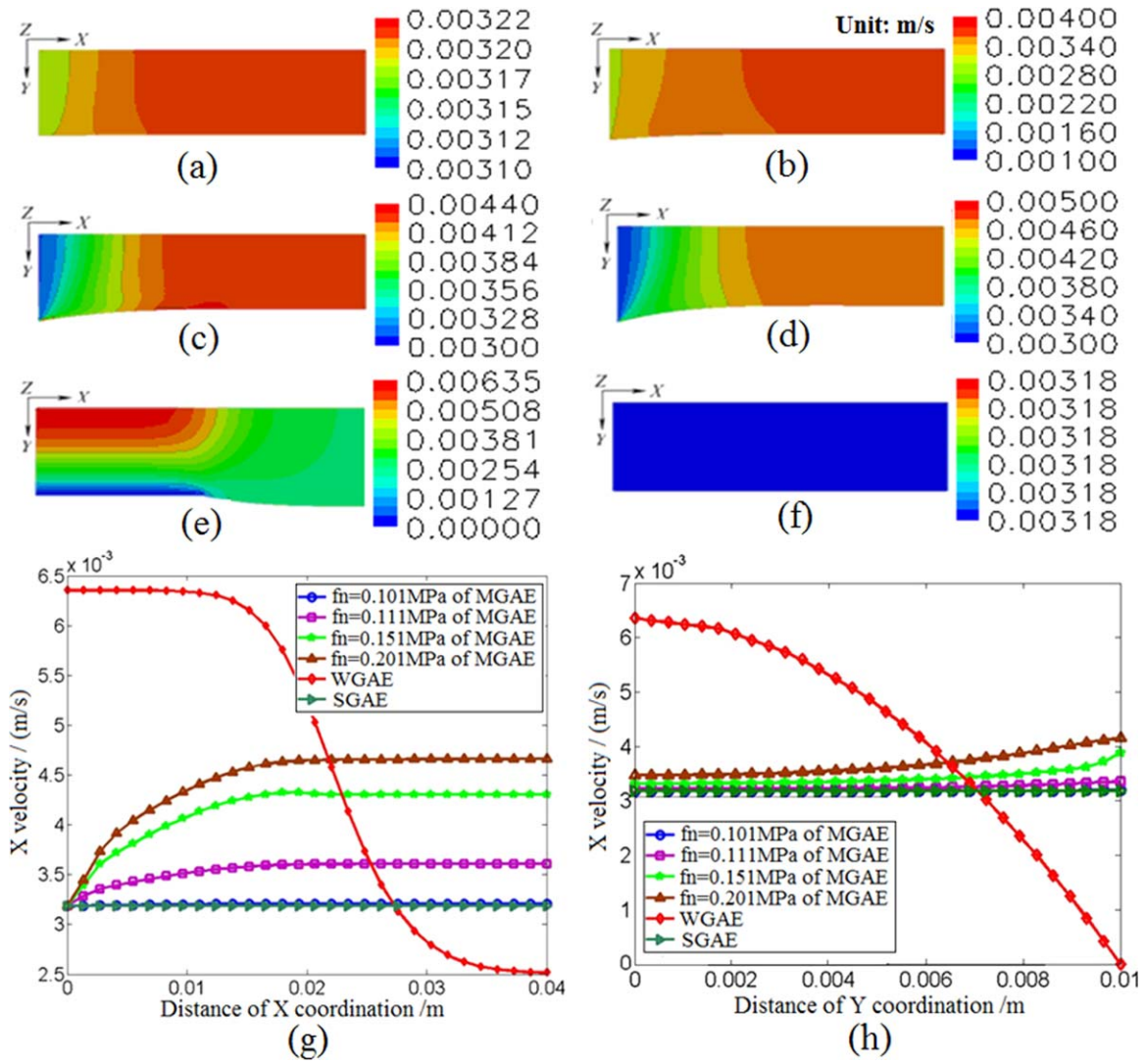

Figure 9. Melt X velocity distributions of MGAE, WGAE, and SGAE. (a) gas pressure is 0.101 MPa,(b) gas pressure is 0.111 MPa, (c) gas pressure is 0.151 MPa, (d) gas pressure is 0.201 MPa, (e) WGAE, (f) SGAE, (g) X velocities along the direction of die channel, and (h) X velocities along the radial direction of die entrance. [Color figure can be viewed in the online issue, which is available at wileyonlinelibrary.com.]

Influence of Gas Pressures on the Pressure Drop of Melt. Figure 11(a–d) shows the melt pressure drop distributions of MGAE under the four different gas pressures. Figure 11(e,f) show the melt pressure drop distributions of WGAE and SGAE. The melt pressure drop changes close to the gas/melt interface for the four MGAEs and close to the die wall for WGAE and SGAE along the die channel direction are shown in Figure 11(g).

From Figure 11(a–d,g), it can be seen that the melt pressure drops are mainly generated adjacent to the gas/melt interface at the die entrance, and the melt pressure drop increases with increasing the gas pressure. But for the WGAE [see Figure 11(e,g)], the melt pressure drop at the die entrance is too much larger than that of MGAE although the melt pressure drop gradually decreases along the direction of die channel. And the melt pressure drop is negative at the wall of die exit, which is generated by the melt extrudate swell effect. For the SGAE [see Figure 11(f,g)], the melt pressure drop isn't generated in the flow field, the result is completely idealized and not agreement with the actual situation.

Influence of Gas Pressures on the First Normal Stress Difference of Melt. Figure 12(a–d) show the first normal stress difference ($N_1 = \tau_{xx} - \tau_{yy}$) distributions of the melt under the influence of four different gas pressures. Figure 12(e,f) show the first normal stress difference distributions of WGAE and SGAE. The first normal stress difference changes of MGAEs, WGAE, and SGAE along the direction of die channel are shown in Figure 12(g).

From Figure12(a–d,g), it can be seen that the first normal stress differences of the four MGAEs are mainly generated adjacent to the gas/melt interface of the die entrance, and increase with increasing the gas pressure. For the WGAE [see Figure 12(e,g)], the first normal stress difference is observed at the wall of the die exit, whereas, in Figure 12(e,g), no first normal stress difference of the SGAE is observed in the whole flow field.

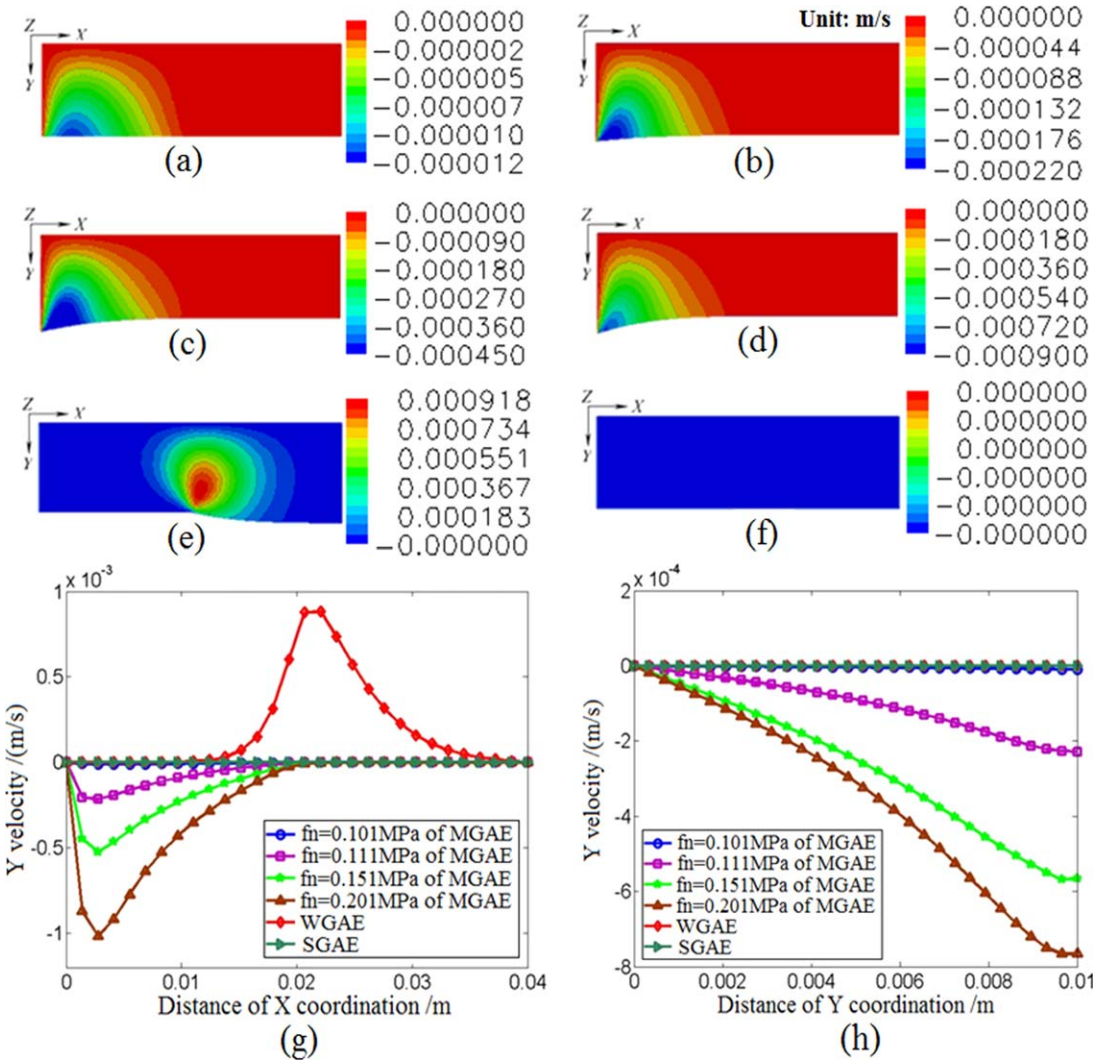

Figure 10. Melt Y velocity distributions of MGAE, WGAE, and SGAE. (a) Gas pressure is 0.101 MPa (b) gas pressure is 0.111 MPa, (c) gas pressure is 0.151 MPa, (d) gas pressure is 0.201 MPa, (e) WGAE, (f) SGAE, (g) Y velocities along the die channel direction, and (h) Y velocities along the radial direction of die entrance. [Color figure can be viewed in the online issue, which is available at wileyonlinelibrary.com.]

Influence of Gas Pressures on the Gas Density. Figure 13(a–d) show the gas density changes for four gas pressures of 0.101, 0.111, 0.151, and 0.201 MPa along the direction of gas channel, respectively.

From Figure 13(a–d), it can be seen that the gas density is not a constant value as like as the incompressible fluid, but increases with increasing the compressible gas pressure. And for each of gas density, the density distribution decreases along the direction of gas channel, that is, the gas density decreases with decreasing the gas pressure. It is demonstrated that gas density has the positive proportion relationship with the gas pressure, which is in good agreement with the ideal gas state equation [see eq. (12)]. And it is also verified that the gas should be regarded as the compressible fluid in the numerical simulation of GAE because the gas density is changed with the position, gas pressure, and temperature.

Discussion

Although the researches of GAE used to overcome some extrudate problems have been reported in past time,[22–30] the reports of the influence of gas on the melt extrudate is very scare. In the literature Ref. 23, the research results demonstrated that the extrudate swell had not completely removed under the gas assistance. And in literature Ref. 31, Arda found that the sharkskin phenomena had not been completely removed by GAE. In this study, in order to investigate the influence of gas on the melt extrusion forming, the GAE experiments were carried out. From the experimental results of Figures 4 and 5, it can be found that although the extrusion effect of the melt is good when the gas pressure is moderate (about 0.1 MPa) (see Figures 4(b) and 5(b)), the extrudate problems (waveness, distortion, and sharkskin surface defect phenomena) become more and more serious with increasing the gas pressure. So, it is demonstrated that the gas pressure has a significant influence on the melt extrusion forming, and the experimental results are in good agreement with the results of Arda.[31]

As we all know, numerical simulation is an efficient way to study the flow behavior and physical field distributions during the process of polymer forming. But in the past reports,[22–31]

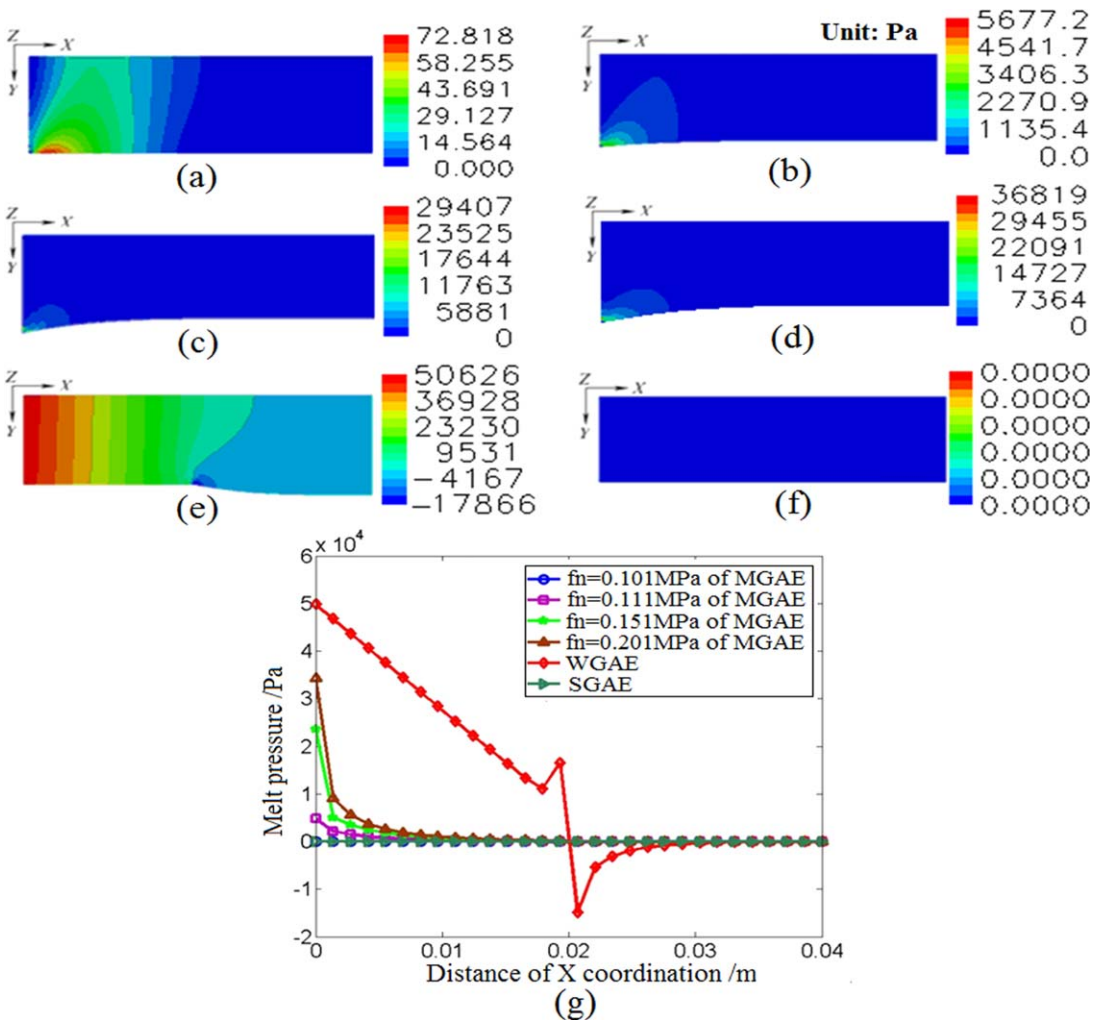

Figure 11. Melt pressure drop distributions of MGAE, WGAE, and SGAE. (a) Gas pressure is 0.101 MPa, (b) gas pressure is 0.111 MPa, (c) gas pressure is 0.151 MPa, (d) gas pressure is 0.201 MPa, (e) WGAE, (f) SGAE, and (g) melt pressure drop change along the direction of die channel. [Color figure can be viewed in the online issue, which is available at wileyonlinelibrary.com.]

the GAE numerical simulation was achieved using the full-slip wall boundary condition and neglected the gas layer and its influence. In this study, in order to further ascertain the influence mechanism of the gas on melt extrusion forming, and to verify the shortcomings of SGAE numerical simulation based on full-slip wall boundary condition, the non-isothermal numerical simulations of the MGAE under the assistance of different gas pressures (i.e. 0.101 MPa, 0.111 MPa, 0.151 MPa, and 0.201 MPa) are studied. According to the real flow characteristics of melt and gas, the gas/melt two-phase fluid model is established, and the changeable density of gas is achieved via the UDF method in finite element software package POLYFLOW. The extrudate profiles, physical distributions (X and Y velocities, pressure drop, and first normal stress difference) are obtained. And the numerical results of MGAE are compared with WGAE and SGAE. From the simulated results of the SGAE based on full-slip wall boundary condition [see Figure 8(b) and 9(f)–12(f)], it can be seen that the physical field distributions (X and Y velocities, pressure drop, and first normal stress difference) are all equal to zero or not changed, this simplified simulation results are not obviously consistent with the actual situation although the seemingly good extruded shape can be obtained. The unrealistic results of the SGAE are generated because the influence of the gas layer on the melt flow behavior is neglected. But for the numerical simulation of MGAE based on gas/melt two-phase fluid model, it can be seen that the numerical results of MGAE are obviously different with that of the SGAE. From the simulated results of melt extruded shape and shrinkage ratio (see Figures 6 and 7), it can be seen that the melt shrinkage ratio increases with increasing the gas pressure. From the simulation results of melt velocity field distributions (see Figures 9 and 10), it can be seen that the melt X and Y velocities increase with the increase of the gas pressure, and for each of gas pressure, the melt X velocity distributions are gradually increased along direction of the die channel. And from the viewpoint of the melt radial velocity distributions, the X and Y velocities close to the gas layer is higher than that of the inner melt, which indicates that the compressible gas has the significant effect on the melt flow velocities. So, in practice, it is desirable to increase the extrusion velocity and volume flow

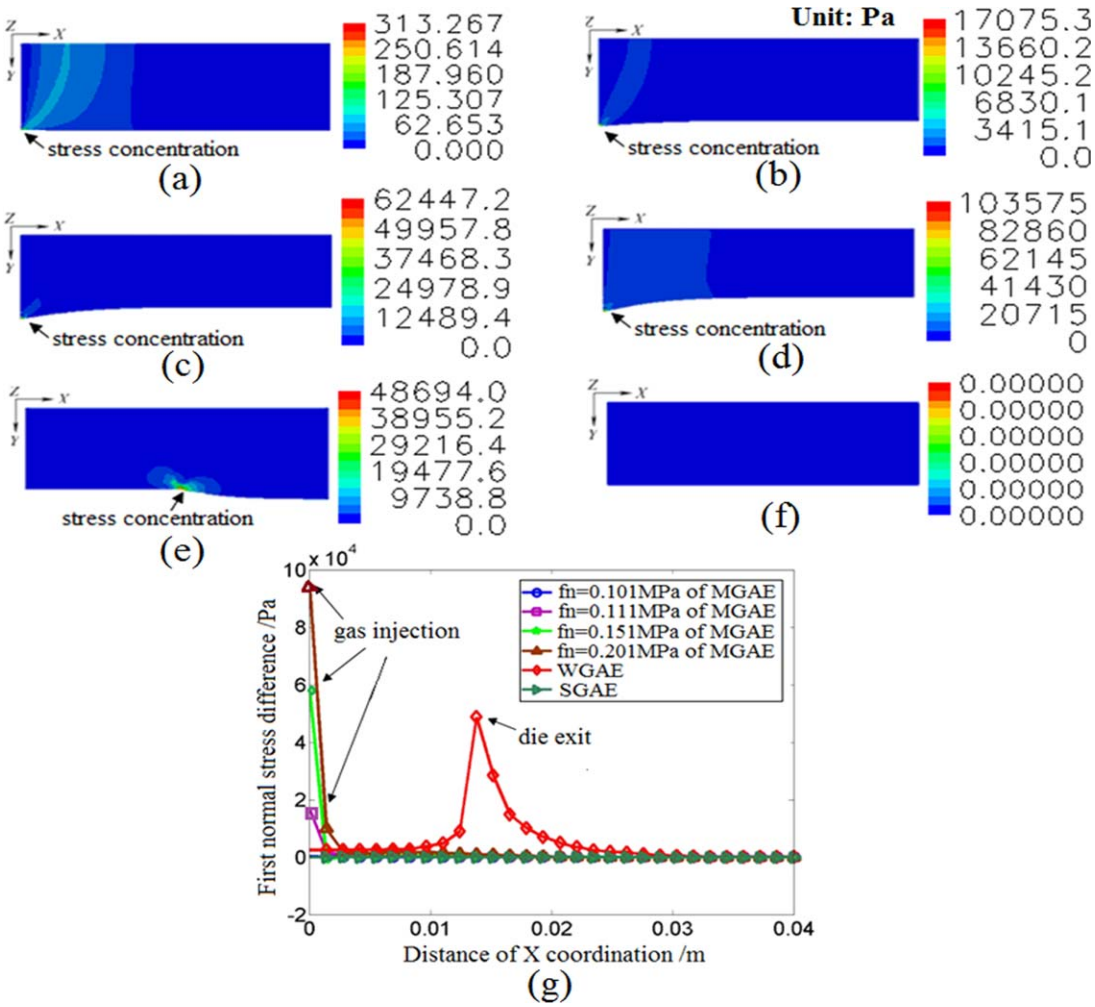

Figure 12. Melt N_1 distributions of MGAE, WGAE, and SGAE. (a) gas pressure is 0.101 MPa, (b) gas pressure is 0.111 MPa, (c) gas pressure is 0.151 MPa, (d) gas pressure is 0.201 MPa, (e) WGAE, (f) SGAE, and (g) melt N_1 changes of along the direction of die channel. [Color figure can be viewed in the online issue, which is available at wileyonlinelibrary.com.]

rate of polymer melt by means of an appropriate increase of gas pressure as long as the melt is not obviously deformed. In addition, for the melt pressure drop and first normal stress difference distributions (see Figures 11 and 12), the melt pressure drop and first normal stress difference are all observed close to the gas/melt interface of die entrance, and these values increase with increasing the gas pressure, these melt pressure drop and first normal stress difference are all induced by the gas pressure, which result in the melt deformation and the increase of the melt velocity. In the literature Ref. 31, Arda revealed that the sharkskin had not been completely removed because the stress concentration was not zero and only transferred from the die exit to the import of gas injection. So, it can be demonstrated that the gas pressure induced first normal stress difference concentration is the main reason of triggering the flow behavior changes, other physical field distributions (X velocity, Y velocity, and pressure drop), the extrudate deformation and sharkskin surface defect phenomena.

From the simulation results of the gas density distribution (see Figure 13), it is demonstrated that the gas is compressible because the gas density is changed with the position, gas pressure, and temperature. In order to interpret the gas is compressible fluid, the mach number can be computed according to the following equation:

$$M_a = \frac{v_{II}}{v_s} \tag{22}$$

where M_a is mach number of fluid, v_{II} is the flow velocity, and v_s is the local sound velocity, which can be gotten using the following equation:

$$v_s = \sqrt{\gamma RT} \tag{23}$$

where γ is the specific heat ratio of gas, for compressible gas, the value of γ can be set to about 1.4, R is the gas constant (287 J/kg·K), and T is the local absolute temperature. According to eq. (23), the local sound velocity is about 436 m/s when local absolute temperature is 473 K.

The axial velocities of gas under the different gas pressures are computed via numerical simulation, which are shown in Figure 14.

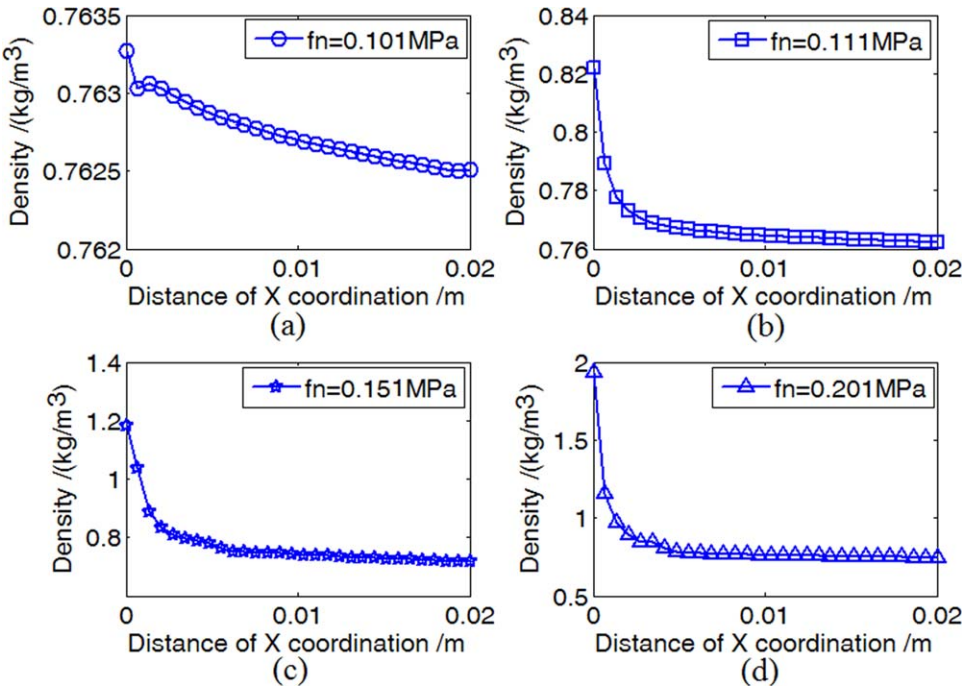

Figure 13. Gas density changes of four different gas pressures along the direction of gas channel. (a) Gas pressure is 0.101 MPa, (b) gas pressure is 0.111 MPa, (c) gas pressure is 0.151 MPa, and (d) gas pressure is 0.201 MPa. [Color figure can be viewed in the online issue, which is available at wileyonlinelibrary.com.]

From Figure 14, it can be seen that the maximum axial velocity of gas reaches 190.71 m/s when the gas pressure is 0.105 MPa, and the maximum axial velocity of gas becomes larger and larger when the gas pressure is increased. According to the gas dynamics, when the mach number of gas flow is larger than 0.3, the gas can be regarded as the compressible fluid. Based on the eq. (22), the mach number of the gas flow with gas pressure of 0.105 MPa, 0.111 MPa, 0.151 MPa, and 0.201 MPa can be computed and are all larger than 0.3. Therefore, in the numerical simulation of GAE, the gas layer should be added into the gas/melt two-phase flow model rather than the full-slip wall boundary condition and the compressibility of gas should also be considered.

In addition, From Figure 9, it can be seen that the increase of gas pressure can improve the extrusion speed, but the melt shape is deformed when the gas pressure is too large (see Figure 6), that is, when the gas pressure is increased in GAE forming, a contradiction exists between the improvement of extrusion velocity and the elimination of shape deformation. It is demonstrated that the appropriate control of the gas pressure is one of the most key steps in the GAE. In the GAE experiments, the melt pressure and the corresponding minimal gas pressure were obtained for the different volumetric flow rate of melt (0.78, 1.13, and 1.45 cm^3/s), which are shown in Figure 15.

From Figure 15, it can be seen that the melt pressure increases with increasing the volumetric flow rate of melt, and the minimal gas pressure should be increased with increasing the volumetric flow rate of melt.

CONCLUSIONS

GAE of polymer melt is a promising forming method of avoiding the extrusion problems because of the gas layer assistance. In this study, the influence of gas pressure on melt extrusion forming was experimentally studied. The experimental results demonstrate that

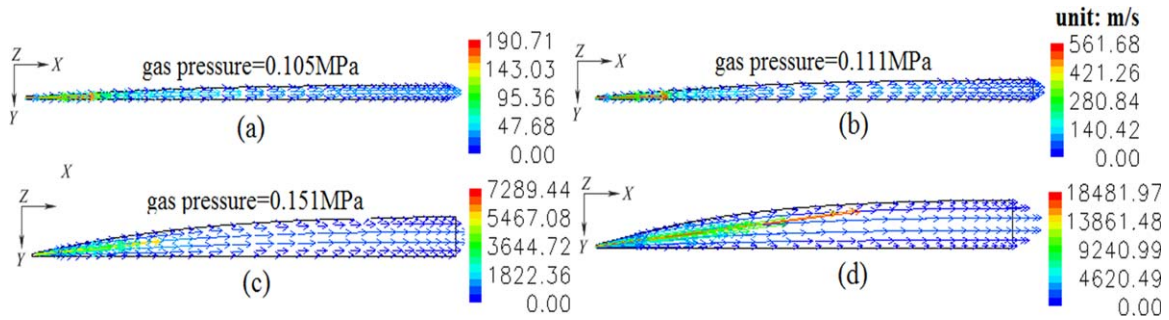

Figure 14. The axial velocities of gas under the different gas pressures. (a) Gas pressure is 0.105 MPa, (b) gas pressure is 0.111 MPa, (c) gas pressure is 0.151 MPa, and (d) gas pressure is 0.201 MPa. [Color figure can be viewed in the online issue, which is available at wileyonlinelibrary.com.]

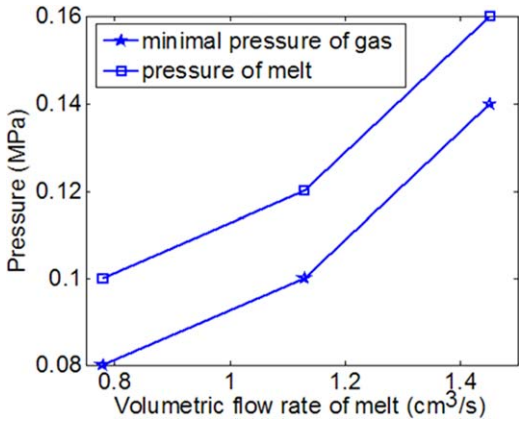

Figure 15. The melt pressures and minimal gas pressures for different volumetric flow rates of melt. [Color figure can be viewed in the online issue, which is available at wileyonlinelibrary.com.]

the extrudate instability and surface sharkskin defect phenomena still exist in GAE, even become more serious with increasing gas pressure. In order to further ascertain the influence mechanism of gas pressure on melt extrusion, the numerical simulation of GAE was also performed. In order to better reflect the influence mechanism of gas on the melt extrusion and to reveal the drawback of the SGAE based on full-slip wall boundary condition usually used in the past time, the non-isothermal numerical simulations of a modified GAE based on gas/melt two-phase flow model are proposed and studied in this study, and the gas compressibility based on changeable density is also considered. Under the influence of different gas pressures, the extruded shape, velocities, pressure drop, and first normal stress difference distributions of the molten polypropylene are obtained and analyzed, as well as the gas density distributions. Numerical results demonstrate that the gas pressure exert great influence on the melt flow behavior in the process of GAE, and the flow behavior, physical field distributions and extrudate shape changes can be well represented by MGAE simulation method rather than SGAE simulation. In addition, the numerical results demonstrate that the gas pressure induced first normal stress difference is the main reason of giving rise to the changes of flow velocities distribution, pressure drop distribution, extrudate shape, and sharkskin surface defects of melt. Therefore, in practice application of GAE, the gas parameters including gas pressure, temperature, and flow rate should be reasonably controlled. In numerical simulation of GAE, the gas layer and its influence on melt extrusion should be taken into account.

ACKNOWLEDGMENTS

This work was supported by the National Natural Science Foundation of China (no. 51163011, 51463015), Doctoral program of Higher Education Research Foundation (no. 20093601110001), and Graduate Innovation Foundation of Jiangxi Province (no. YC2014-B004).

REFERENCES

1. Tadmor, Z.; Klein, I. Engineering Principles of Plasticating Extrusion; Wiley-Inter-Science: New York, **1970**.
2. Liu, X. Q.; Li, K.; McAfee, M.; Nguyen, B. K.; McNally, G. M. *Polym. Eng. Sci.* **2012**, *52*, 6.
3. Lee, S. T. *J. Cell. Plast.* **2010**, *46*, 321.
4. Wu, X. H.; Zhao, G. Q.; Luan, Y. G.; Ma, X. W. *Mater. Sci. Eng. A* **2006**, *435–436*, 266.
5. Pirkle, J. C., Jr.; Braatz, R. D. *J. Rheol.* **2010**, *54*, 471.
6. Abrinia, K.; Ghorbani, M. *Mater. Manuf. Processes* **2012**, *27*, 420.
7. Graessley, W. W.; Glasscock, S. D.; Crawley, R. L. *J. Rheol.* **1970**, *14*, 519.
8. Tanner, R. I. *J. Polym. Sci., Part B: Polym. Phys.* **1970**, *8*, 2067.
9. Liang, J. Z. *Polym. Test* **2008**, *27*, 936.
10. Mitsoulis, E.; Georgiou, G. C.; Kountouriotis, Z. *Comput. Fluids* **2012**, *57*, 195.
11. Tzoganakis, C.; Price, B. C.; Hatzikiriakos, S. G.; Tzoganakis, C. *J. Rheol.* **1993**, *37*, 355.
12. Burghelea, T. I.; Griess, H. J.; Münstedt, H. *J. Non-Newton. Fluid Mech.* **2010**, *165*, 1093.
13. Ganß, M.; Satapathy, B. K.; Thunga, M.; Weidisch, R.; Pötschke, P.; Jehnichen, D. *Acta Mater.* **2008**, *56*, 2247.
14. Robert, L.; Vergnes, B.; Demay, Y. *J. Non-Newton. Fluid Mech.* **2003**, *112*, 27.
15. Musil, J.; Zatloukal, M. *Chem. Eng. Sci.* **2010**, *65*, 6128.
16. Sakharov, A. S.; Sivetskii, V. I.; Sokolskii, A. L. *Chem. Pet. Eng.* **2011**, *47*, 231.
17. Yang, C.; Li, Z. R. *Polym. Test.* **2014**, *37*, 45.
18. Dubrocq-Baritaud, C.; Darque-Ceretti, E.; Vergnes, B. *J. Non-Newton. Fluid Mech.* **2011**, *166*, 847.
19. Ismail, H.; Zaaba, N. F. *Polym. Plast. Technol. Eng.* **2011**, *50*, 1214.
20. Gunes, K.; Isayev, A. I. *Polym. Sci. Ser. A* **2010**, *52*, 1124.
21. Panov, A. A.; Anasova, T. A.; Zaikov, G. E.; Panov, A. K. *Theor. Found. Chem. Eng.* **2011**, *45*, 436.
22. Brzoskowski, R.; White, J. L.; Szydlowski, W.; Weissert, F. C.; Nakajima, N.; Min, K. *Rubber Chem. Technol.* **1987**, *60*, 945.
23. Liang, R. F.; Mackley, M. R. *J. Rheol.* **2001**, *45*, 211.
24. Kamişli, F.; Ryan, M. E. *Int. J. Numer. Methods Fluids* **2002**, *38*, 407.
25. Huang, X. Y. *PhD Dissertation;* Nanchang University: Nanchang, China, **2006**.
26. Huang, X. Y.; Liu, H. S.; Zhou, G. F.; Luo, Z. M.; Li, K. S. *J. Plast. Eng. (China)* **2005**, *12*, 101.
27. Liu, H. S.; Lu, C.; Huang, X. Y.; Deng, X. Z. *J. Plast. Eng. (China)* **2008**, *15*, 158.
28. Xiao, J. H.; Liu, H. S.; Huang, X. Y.; Xiong, A. H. *Polym. Mater. Sci. Eng. (China)* **2009**, *25*, 167.
29. Huang, Y. B. PhD Dissertation, Nanchang University: Nanchang, China, **2011**.
30. Deng, X. Z. PhD Dissertation, Nanchang University: Nanchang, China, **2014**.
31. Arda, D. R.; Mackley, M. R. *Rheol. Acta* **2005**, *44*, 352.
32. ANSYS. ANSYS POLYFLOW 14.5 User's Guide, ANSYS., Southpointe, **2012**.
33. Thien, N. P.; Tanner, R. I. *J. Non-Newton Fluid. Mech.* **1977**, *2*, 353.